Article

Experimental study on the damage process of marble under true triaxial pre-peak unloading conditions

Yaohui Gao[1] and Zhaofeng Wang[2,3]

Abstract

Stress-induced instability is associated with rock damage. Here, the progressive brittle fracturing process in Jinping marble is studied by introducing two types of true triaxial pre-peak unloading tests, namely, the incrementally cyclic loading-unloading minimum principal stress test (ICM test) and the incrementally cyclic loading-unloading maximum and minimum principal stress test (ICMM test). By comprehensively analysing the irreversible strains, dissipated energy, acoustic emission (AE) characteristics and scanning electron microscopy (SEM) results, the rock damage evolution can be quantified and divided into two distinctive damage stages. At the boundary point, the irreversible strain increments reach their minimum values. In the gentle damage stage, the normalized irreversible strains increase linearly, and this process is associated with a small number of AE hits with low amplitude. The rapid damage stage is characterized by a nonlinear increase in the normalized irreversible strains, and this process is associated with a large number of AE hits with high amplitude. The dissipated energy mainly increases in the rapid damage stage. In addition, the rapid damage stage in the ICMM test mainly occurs in the last five cycles, due to the differences in the deviatoric stresses in each cycle. In both of these tests, the failure mode is principally characterized by tensile failure. Moreover, the precursory signals of rock fracturing and the influence of the loading paths on the strength are discussed.

[1]PowerChina Huadong Engineering Corporation Limited, Hangzhou, China
[2]State Key Laboratory of Geomechanics and Geotechnical Engineering, Institute of Rock and Soil Mechanics, Chinese Academy of Sciences, Wuhan, China
[3]University of Chinese Academy of Sciences, Beijing, China

Corresponding author:
Zhaofeng Wang, State Key Laboratory of Geomechanics and Geotechnical Engineering, Institute of Rock and Soil Mechanics, Chinese Academy of Sciences, Wuhan 430071, China.
Email: zfwang@whrsm.ac.cn

Introduction

In deeply-buried hard rock with high in situ stresses, stress-induced failure after tunnel excavation is primarily responsible for tunnel instability. Based on extensive field investigations performed using state-of-the-art techniques and instruments, some typical brittle failure modes, such as spalling and rockbursts, have been recorded (Feng et al., 2016a, 2018). The occurrence of spalling or rockburst events is an evolving damage process mainly associated with sufficient energy conversion and rock damage in a local failure zone (Ortlepp and Stacey, 1994).

Taking rockburst as an example, the mechanism of rockburst evolution can be divided into four processes: stress adjustment, energy accumulation, crack development and the collapse and ejection of fractured rocks (Li et al., 2012; Su et al., 2019). The extent of rock damage plays a prominent role in determining failure patterns and intensity. On the other hand, rock damage mechanisms involve the initiation, propagation and coalescence of microcracks. These rock cracking and fracturing processes have been studied both experimentally and theoretically for many years (Brace et al., 1966; Cai, 2008; Diederichs et al., 2004; Eberhardt et al., 1998; Gao et al., 2010; Li et al., 2018; Liu et al., 2018; Liu and Xu, 2015; Lockner et al., 1991; Martin and Chandler, 1994). These studies have contributed to a better understanding of the mechanical properties of stress-induced failure. Moreover, to quantify the progression of brittle fracturing, a large number of cyclic loading and unloading tests have been conducted. For instance, Martin and Chandler (1994) and Eberhardt et al. (1999) identified and characterized brittle fracture processes using several damage-controlled uniaxial compression tests. Qiu et al. (2014) quantified irreversible strains during pre-peak unloading damage evolution under triaxial cyclic loading and unloading tests. In addition, Liang et al. (2017) investigated the characteristic features of rock during the post-peak stage under loading and unloading confining pressure conditions. By establishing a relationship between accumulative damage and the corresponding stress conditions, it is possible to develop a damage model of rock material (Feng and Yu, 2010; Liu and Xu, 2015; Liu et al., 2018).

However, the rock mass surrounding a deep tunnel is subjected to a three-dimensional stress state before excavation. After excavation, the stress concentration near the excavation boundary is significant. Although the true stress paths in underground tunnels are complex, some typical loading and unloading paths correspond to stress redistribution (Feng et al., 2020). More specifically, the radial stress (minimum principal stress) decreases whereas the tangential stress (maximum principal stress) increases, and the stress parallel to the tunnel axial direction (intermediate principal stress) remains nearly constant. Moreover, a stress path in which only the minimum principal stress decreases also occurs. Therefore, it is necessary to perform true triaxial tests in which the stress paths can approximate the stress concentration to better investigate the damage evolution due to the in situ stress-induced brittle instability. Recently, due to the development of true triaxial apparatuses and associated auxiliary monitoring instruments, such as optical microscopes, scanning electron microscopes (SEM), high-speed cameras and acoustic emission (AE) monitoring equipment, it has been possible to study brittle rock failure processes under true triaxial loading and unloading conditions. For instance, Mogi (1972) studied the influence of the intermediate principal stress on the strength, ductility, stress drop and fracturing of rock. Haimson (2007) established the micromechanisms of borehole breakout failure using vertical borehole drilling experiments. He et al. (2010) studied the rockburst process in limestone and its corresponding AE characteristics. Du et al. (2016) observed the spalling and rockburst induced by true triaxial unloading and local dynamic disturbances. In addition, Tiwari and Rao (2007) investigated the influence of joints on the strength and failure characteristics of rock under polyaxial stress states. In short, these experimental studies focused on the stress-induced brittle fracturing process with the aid of high-speed

cameras and AE monitoring instruments. However, the energy and deformation characteristics of stress-induced brittle failure under true triaxial loading and unloading conditions were not assessed in detail.

In this paper, two types of damage-controlled tests were carried out under true triaxial cyclic loading and unloading conditions to estimate the progressive failure of Jinping marble. AE and SEM technology were also employed to record the stress-induced brittle fracturing process and investigate the failure patterns, respectively. Based on the characteristics of the AE results, the recorded irreversible strains and the calculated dissipated energy, different damage stages were established to describe the damage evolution. The damage precursor of rock fracturing and the influence of stress paths on the strength of Jinping marble were also discussed.

Experimental material, apparatus and procedures

Project background and rock specimens

This study is based on the second phase of the Chinese Jinping Underground Laboratory project (CJPL-II) in Sichuan Province, southwestern China. The Chinese Jinping Underground Laboratory (CJPL) is located at a depth of approximately 2400 m in the Jinping Mountains. It is currently one of the world's deepest laboratories (Feng et al., 2016a) and thus experiences very high in situ stresses. Feng et al. (2016a) described the project background in further detail. The in situ stress was measured using the stress relieving method, and the approximate maximum, intermediate, and minimum principal stresses were evaluated to be 70 MPa, 60 MPa and 30 MPa, respectively. In this underground engineering area, tunnel excavation causes the redistribution of the in situ stresses in the surrounding rock. Moreover, due to the partial excavation method, the surrounding rock experiences complex loading and unloading processes.

The marble specimens used in the true triaxial tests were taken from laboratory #7. The tested marble specimens are grey-white and belong to the Triassic Baishan group (T_2b). The mineral contents of these rectangular prismatic specimens (50 mm × 50 mm × 100 mm) primarily comprise dolomite (approximately 90%) and calcite (nearly 10%).

True triaxial loading apparatus

The experiments in this study were carried out using Northeastern University's true triaxial apparatus (TTA), as shown in Figure 1. Feng et al. (2016b) presented its capability and main parameters in detail. Feng et al. (2017) also evaluated the end friction effect and suggested the use of the anti-friction agent MSV (a mixture of stearic acid and Vaseline at a 1:1 mass ratio) in both true triaxial tests and conventional triaxial tests. Thus, the deformations in the three principal stress directions were accurately measured. Additionally, AE signals were monitored throughout loading and unloading processes.

Testing programme

To obtain the characteristic stress levels in the true triaxial unloading tests, the corresponding true triaxial loading tests were first conducted. Figure 2(a) shows the loading stress path, that is, the first stress path, in which the maximum principal stress is generally varied using the strain control while the predefined intermediate and minimum principal stresses are held constant until reaching the residual stage or failure. Figure 2(b) shows the stress path of the incrementally cyclic loading-unloading minimum principal stress test (called the ICM test), namely, the second stress path, in
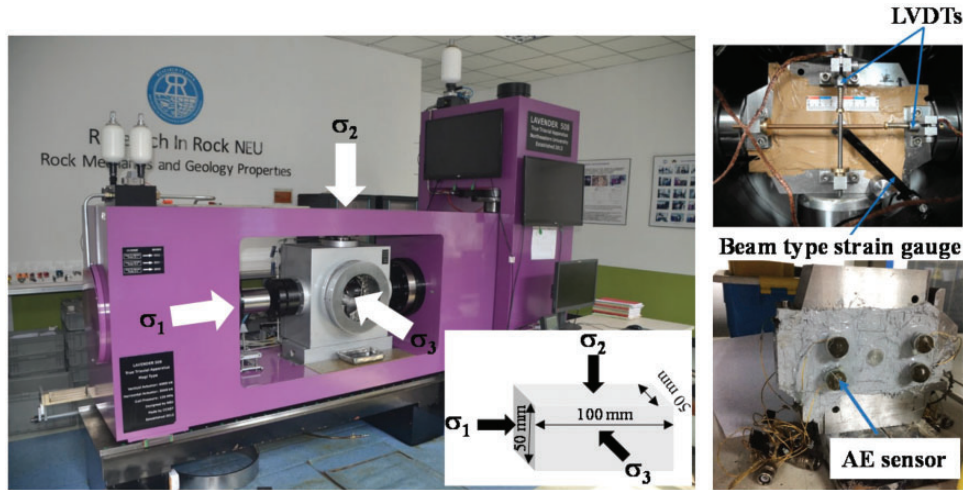
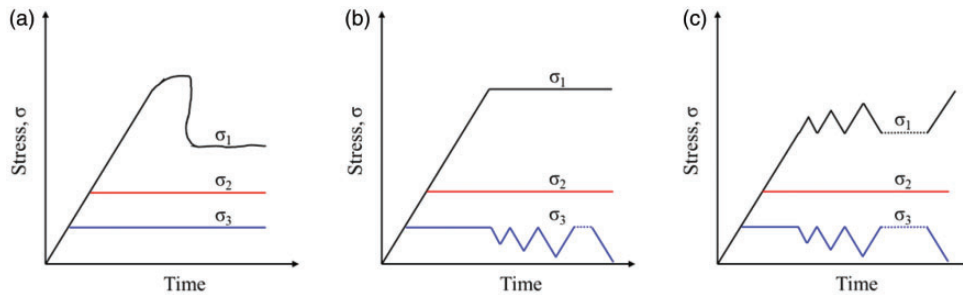**Figure 1.** Schematic diagram of the test machine (after Feng et al. 2016b)

Figure 2. Schematic diagram of the stress paths: (a) first path, (b) second path, and (c) third path. In the second and third paths, the dash line represents the omitted unloading and reloading cycles.

which the minimum principal stress is loaded and unloaded repeatedly while the other predetermined principal stresses remain constant until failure. As shown in Figure 2(c), the third stress path (called the ICMM test) involves incrementally unloading and loading the minimum and maximum principal stresses simultaneously until failure while holding the predetermined intermediate principal stress constant.

Test results

Rock damage can be quantified by accumulative irreversible strains, AE events and accumulative dissipated energy (Eberhardt et al., 1999; Iturrioz et al., 2014; Ju et al., 2012; Qiu et al., 2014). For instance, Eberhardt et al. (1999) quantified the stresses, strains and AE rates under uniaxial cyclic damage-controlled tests to investigate the stress-induced brittle fracturing damage in the pink Lac du Bonnet. Additionally, Qiu et al. (2014) demonstrated that pre-peak normalized irreversible strains could be divided into a linear steady stage and a nonlinear unstable stage under conventional

triaxial cyclic loading and unloading conditions. Carpinteri et al. (2016) also discussed the relationship between the AE emitted energy, the dissipated energy and the fracture energy. The descriptions of rock damage adopted by Eberhardt et al. (1999) and Qiu et al. (2014) are introduced below:

$$D_1 = \frac{\sum_{j=1}^{i} (\varepsilon_1^p)_j}{\sum_{i=1}^{n} (\varepsilon_1^p)_i} \tag{1}$$

$$D_2 = \frac{\sum_{j=1}^{i} (\varepsilon_2^p)_j}{\sum_{i=1}^{n} (\varepsilon_2^p)_i} \tag{2}$$

$$D_3 = \frac{\sum_{j=1}^{i} (\varepsilon_3^p)_j}{\sum_{i=1}^{n} (\varepsilon_3^p)_i} \tag{3}$$

$$D_v = \frac{\sum_{j=1}^{i} (\varepsilon_v^p)_j}{\sum_{i=1}^{n} (\varepsilon_v^p)_i} \tag{4}$$

$$D_e = \frac{\sum_{j=1}^{i} (U_d)_j}{\sum_{i=1}^{n} (U_d)_i} \tag{5}$$

$$D_{AE} = \frac{\sum_{j=1}^{i} (N)_j}{\sum_{i=1}^{n} (N)_i} \tag{6}$$

$$D_\sigma = \frac{\sum_{j=1}^{i} (\Delta\sigma)_j}{\sum_{i=1}^{n} (\Delta\sigma)_i} \tag{7}$$

where D_1, D_2, D_3, D_v, D_e, D_{AE} and D_σ are the damage variables for the maximum principal strain, intermediate principal strain, minimum principal strain, volumetric strains, accumulative dissipated energy, accumulative AE hits and stress changes, respectively; ε_1^p, ε_2^p, ε_3^p, ε_v^p, U_d, N and $\Delta\sigma$ are the irreversible maximum principal strain, intermediate principal strain, minimum principal strain, volumetric strain, accumulative dissipated energy, accumulative AE hits and changes in stress in an individual cycle, respectively; i is the number of cycles; j is summed from the first cycle to the i-th cycle and n is the total number of cycles. Gao and Feng (2019) studied the relations between some of the abovementioned damage variables and the critical equivalent irreversible strain.

The relationships derived from these seven damage parameters are investigated for two different stress paths: (i) the incrementally cyclic loading-unloading the minimum principal stress solely (ICM test) and (ii) the incrementally cyclic loading-unloading the minimum and maximum principal stresses simultaneously (ICMM test). Note that the predetermined maximum principal stresses at the beginning of the first unloading cycle in these two tests fall below the corresponding crack damage threshold σ_{cd} which is defined as the stress corresponding to the reversal point in the maximum principal stress and total volumetric strain curve. Additionally, σ_{cd} represents the stress level that controls the unstable crack development of the rock material and is regarded as the rock long-term strength.

True triaxial loading tests

To determine the initial stress levels in the following cyclic loading and unloading tests and investigate the influence of the stress path on the rock damage, true triaxial loading tests are conducted first such that the corresponding characteristic stress levels can be acquired. This process guarantees that the specimens not only initially suffer minimum damage but also eventually fail under the predetermined stress conditions in the subsequent cyclic loading and unloading tests. The complete deviatoric stress-strain curves and corresponding AE testing results of the specimens in the loading tests are shown in Figure 3.
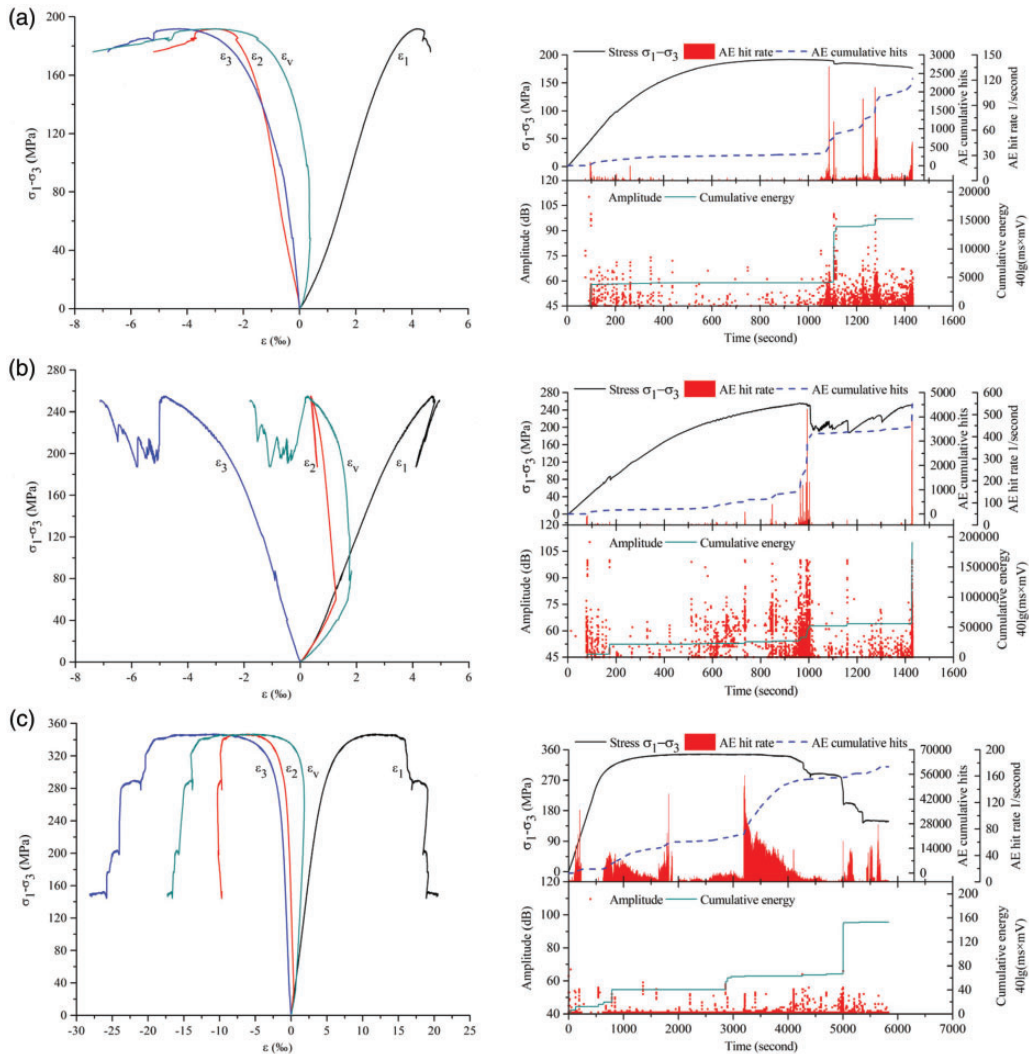

Figure 3. The deviatoric stress-strain curves and corresponding AE results of tested specimens in the loading tests. (a) $\sigma_2 = 0$ MPa, and $\sigma_3 = 0$ MPa, (b) $\sigma_2 = 60$ MPa, and $\sigma_3 = 0$ MPa, and (c) $\sigma_2 = 60$ MPa, and $\sigma_3 = 30$ MPa.

Under different loading conditions, the complete deviatoric stress-strain curves of these specimens can be divided into four phases: the initial compression phase, the elastic deformation phase, the strain hardening phase, and finally the post-peak failure phase. The initial compression phase is related to the concave segment in the complete stress-strain curve, which indicates that the original cracks in the rock specimens are compacted. The elastic deformation phase corresponds to the constant slope of the stress-strain curve, which reflects that no new cracks occur in the rock specimens. The strain hardening phase is associated with the convex section in the complete stress-strain curve and is the result of microcrack propagation. The post-peak failure phase represents the stress-strain curve after the peak stress. Although all four phases are accompanied by AE events (Zhao et al. 2018), AE events mainly occur in the strain hardening phase and the post-peak failure stage. During these stages, cracks initiate, interact, coalesce and gradually form macroscopic failure planes. In addition, the pre-existing cracks in a rock specimen are closed in the initial compression phase, producing a reasonable number of AE events. As shown in Figure 3, the minimum principal stress plays a crucial role in the characteristics of the deviatoric stress-strain curves. When the minimum principal stress is equal to 0 MPa (see Figure 3(a) and (b)), which is regarded as the loading condition at the tunnel boundary (Cai, 2008; Gao et al., 2018; Kong et al., 2018), these curves can be evaluated as reflecting linear-elastic brittle behaviour. Moreover, a ductile plateau emerges as the minimum principal stress increases (see Figure 3(c)).

Incrementally cyclic loading/unloading the minimum principal stress solely (ICM test)

In the first damage-controlled test, the Jinping marble specimen is loaded to the predetermined stress state ($\sigma_1 = 280$ MPa, $\sigma_2 = 60$ MPa, and $\sigma_3 = 30$ MPa) at which σ_1 is less than σ_{cd} (σ_{cd} is approximately 290 MPa, which corresponds to the reversal point in the volumetric strain in Figure 3(c)). While σ_1 and σ_2 remain constant, σ_3 is then unloaded and loaded cyclically at a rate of 0.2 MPa/s. In the first unloading and loading cycle, σ_3 is reduced to 24 MPa and then reloaded to 30 MPa; in the second cycle, σ_3 is unloaded to 20 MPa and then reloaded to 30 MPa; in the following cycles, σ_3 decreases to the value that is 2 MPa less than that in the former unloading cycle and then increases to 30 MPa (see Figure 4(a)). This process is repeated until the specimen fails in the tenth cycle, in which σ_3 is unloaded to 3.44 MPa for specimen B1 and in the twelfth cycle, in which σ_3 is unloaded to 0.05 MPa for specimen B3. In this section, the typical results of specimen B1 are mainly used to introduce the characteristics of the irreversible strains, dissipated energy, AE events and brittle failure in the ICM test.
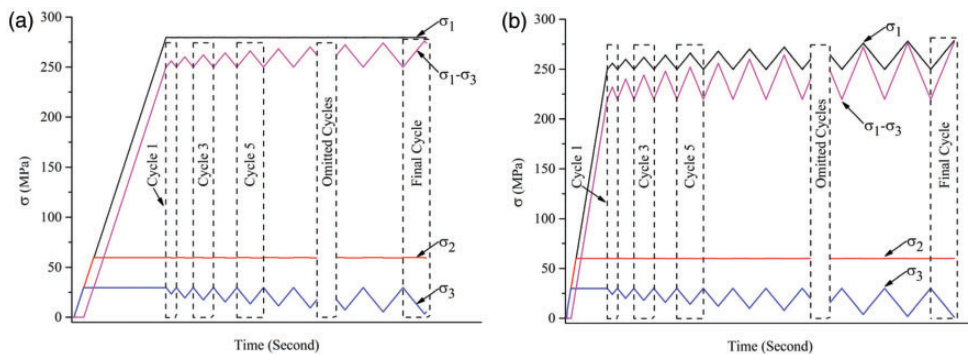

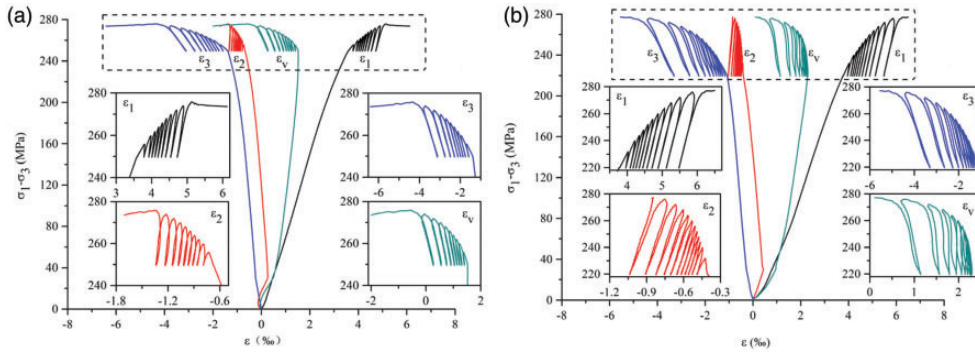**Figure 4.** Schematic diagram of the testing stress path. (a) ICM test and (b) ICMM test.

Figure 5. The deviatoric stress-strain curves in the incrementally cyclic loading/unloading test. (a) ICM test and (b) ICMM test.
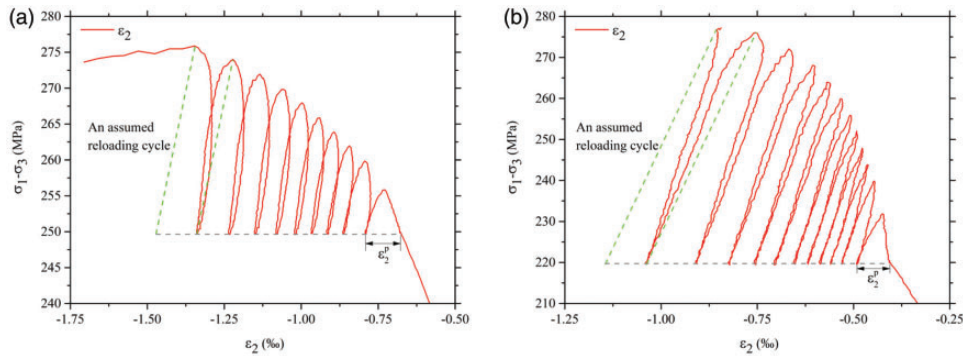

Figure 6. The approach of calculating irreversible strains at the ultimate loading stage using an assumed reloading cycle, which is presented by the green dashed line. (a) ICM test and (b) ICMM test.

Figure 5(a) shows the relationship between the deviatoric stresses (σ_1-σ_3) and strains (ε_1, ε_2, ε_3 and ε_v) of specimen B1. Due to the usage of the stress control method, the specimen fails violently once the load exceeds its bearing capacity. Hence, the reloading displacement cannot be recorded in the final loading cycle. To evaluate the elastic and plastic parameters in the ultimate loading stage, the assumption that these factors, such as Young's modulus and Poisson's ratio, are the same as those in the previous reloading cycle is introduced. Figure 6(a) illustrates the results obtained using this assumed reloading cycle, which is represented by the green dashed line in the intermediate principal strain ε_2.

In each cycle, the loading and unloading curves can be used to obtain the irreversible strains, dissipated energy and AE events. Then, these parameters are normalized to investigate the rock damage evolution. As shown in Figure 7(a), all of the normalized damage parameters exhibit monotonic increasing trends. An exponential function is found to describe the relations among the damage variables, and is defined as follows:

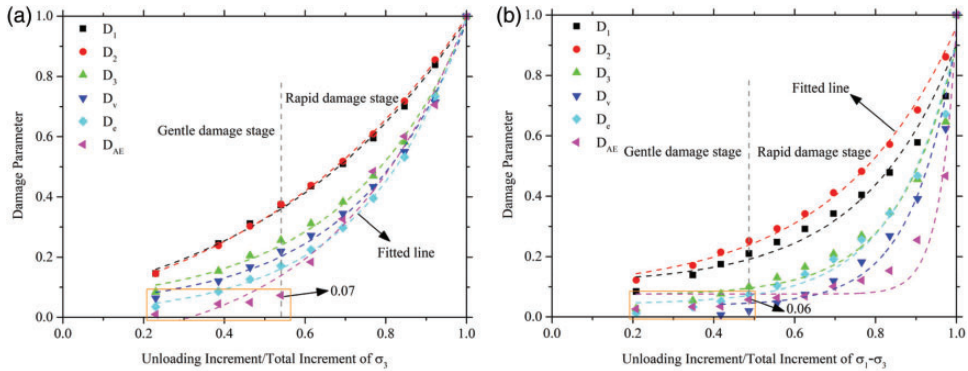$$D = a\exp\left(\frac{-D_\sigma}{b}\right) + c \tag{8}$$

Figure 7. The damage evolution of six damage parameters during the damage process. (a) Specimen B1 in the ICM test and (b) Specimen B32 in the ICMM test.

Table 1. Empirical coefficients in the fitted relations between the damage variables and the stress increment.

Test type	Damage variables	Empirical coefficients			R^2
		a	b	c	
ICM	D_1	0.1602	0.5246	−0.0891	0.9980
	D_2	0.1951	0.5666	−0.1432	0.9993
	D_3	0.0341	0.3011	0.0340	0.9953
	D_v	0.0235	0.2702	0.0284	0.9958
	D_e	0.0191	0.2530	−3.9733E-4	0.9993
	D_{AE}	0.0532	0.3268	−0.1390	0.9804
ICMM	D_1	0.0098	−0.2272	0.1080	0.9624
	D_2	0.0301	−0.2964	0.0830	0.9934
	D_3	7.6770E-4	−0.1432	0.0724	0.9573
	D_v	9.1152E-5	−0.1089	0.0377	0.9674
	D_e	0.0012	−0.1511	0.0425	0.9710
	D_{AE}	2.5858E-11	−0.0412	0.0761	0.9610

ICM: incrementally cyclic loading-unloading minimum principal stress; ICMM: incrementally cyclic loading-unloading maximum and minimum principal stress test.

where D refers to the damage parameter (D_1, D_2, D_3, D_v, D_e and D_{AE}) in equations (1) to (6), and D changes from 0 to 1. Specifically, $D = 0$ means that rock specimen undergoes no damage. $D = 1$ indicates that the rock specimen fails; a, b and c are empirical constants. Table 1 reports the values of the fitted parameters in equation (8). From the viewpoint of the correlation coefficient ($R^2 > 0.95$), equation (8) provides a satisfactory fit to the results. In addition, equation (8) goes through two distinct points, (0, D_0) and (1, 1). Thus, the fitted parameters can be linked together as follows:

$$D_0 = a + c \qquad (9)$$

$$1 = a\exp\left(\frac{-1}{b}\right) + c \tag{10}$$

where D_0 is the initial damage value for the damage parameter. In theory, D_0 should be zero. However, the rock specimen experiences a loading step before the unloading and loading cycles so that the rock specimen will undergo a small initial damage D_0.

To better investigate the whole damage process, Figure 8(a) shows the increments of ε_1^p, ε_2^p, ε_3^p, ε_v^p and U_d in each cycle. Note that the irreversible strain increments exhibit the two opposite change trends in the ICM test. All of the irreversible strain increments decrease before increasing, and the boundary line is represented by the dashed line in Figure 8(a). At this boundary line, the irreversible strain increments reach their minimum values. Therefore, on one hand, when the irreversible strain increments exhibit a downward trend, the rate of the generation of the irreversible strains decreases. In addition, the dissipated energy increments remain nearly constant, and their magnitudes are small. This behaviour indicates that rock specimen experiences a gentle damage evolution in this period. On the other hand, when the irreversible strain increments exhibit an upward trend, the
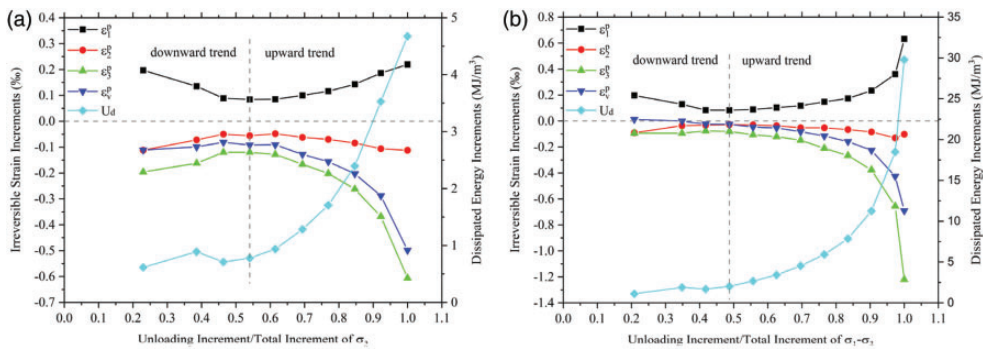

Figure 8. Relationship between the absolute permanent strains, dissipated energy and the damage increment. (a) ICM test and (b) ICMM test.
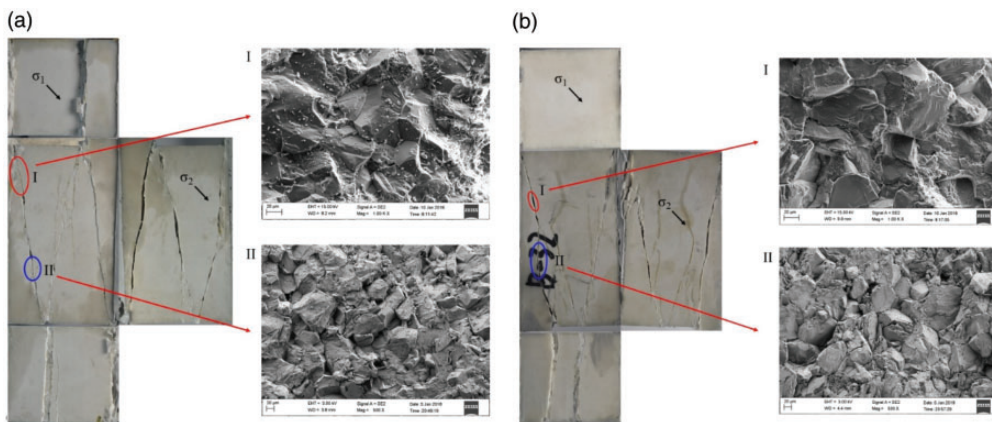

Figure 9. The failure photos and SEM results. (a) ICM test and (b) ICMM test.

accumulation of the irreversible strains increases rapidly. Moreover, the dissipated energy increments also begin to surge. This behaviour indicates that the rock specimen undergoes rapid damage evolution. Additionally, the increments of ε_2^p are very small in all cycles, which is due to the macro-failure plane parallel to the σ_2 direction in the true triaxial tests (see Figure 9(a)). In Figure 9(a), the failure plane features numerous trans-granular and inter-granular fractures, which indicates that the failure pattern of the specimen B1 is mainly tensile.

It is noted in Figure 7(a) that the evolution of the normalized damage parameters also exhibits two different stages, with the same boundary line as shown in Figure 8(a). In the gentle damage stage, the damage parameters (D_1, D_2, D_2, D_v and D_e) increase linearly, and their increase rates are nearly equal. Importantly, the value and increase rate of D_{AE} are small. At the boundary line, the value of D_{AE} is only 0.07, which also validates the correctness and rationality of the different damage evolution stages. In the rapid damage stage, all of the damage parameters increase rapidly and nonlinearly.

To further illustrate the damage evolution in the ICM test, Figure 10(a) presents the properties of AE events for the specimen B1, such as the AE hit rate, cumulative AE hits, amplitude and cumulative energy. In the gentle damage stage, the rock specimen produces few irreversible strains and releases little energy, which corresponds to a slight increase in the number of AE events with low amplitude (Eberhardt et al., 1998). However, in the rapid damage stage, very large irreversible strains and a considerable amount of dissipated energy are generated, thus leading to a prominent rise in the AE hit rate and cumulative AE hits. This stage is characterized by the large amplitude and high cumulative energy of the AE events.

Incrementally cyclic loading/unloading the minimum and maximum principal stresses simultaneously (ICMM test)

To make the stress state in the final cycle equal to the predetermined stress state in ICM test, the Jinping marble specimen is first loaded to the initial stress state ($\sigma_1 = 250$ MPa, $\sigma_2 = 60$ MPa, and $\sigma_3 = 30$ MPa) in the second damage-controlled test (ICMM test). Then, under a constant σ_2, σ_1 and σ_3 are unloaded and reloaded cyclically at the same rate of 0.1 MPa/s. Although the variation in σ_3 in each cycle is the same as that in the first damage-controlled test (ICM test), the ICMM test also simultaneously alters σ_1. More specifically, in the first cycle, σ_1 is loaded to 256 MPa and then reduced to 250 MPa; in the second cycle, σ_1 is reloaded to 260 MPa and then decreased to 250 MPa; in the following cycles, σ_1 increases to a value that is 2 MPa greater than that in the former loading
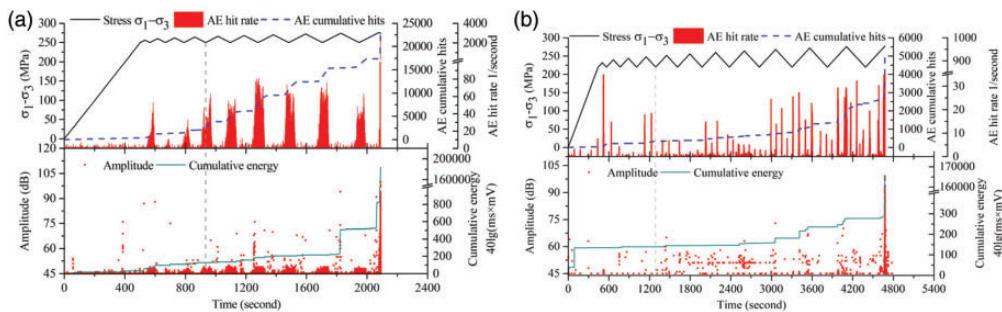

Figure 10. The complete deviatoric stress-time curve and corresponding AE event properties. (a) ICM test and (b) ICMM test.

cycle and then decreased to 250 MPa (see Figure 4(b)). This process is then repeated until failure. Specimen B32 failed in the twelfth cycle, in which σ_3 was unloaded to 1.23 MPa and σ_1 was loaded to 278.44 MPa, and specimen B27 failed in the eleventh cycle, in which σ_3 was unloaded to 1.90 MPa and σ_1 was loaded to 277.86 MPa. In this section, the typical results of specimen B32 are used to introduce the characteristics of the irreversible strains, dissipated energy, AE events and brittle failure in the ICMM test.

Figure 5(b) shows the deviatoric stress-strain curve of specimen B32. Additionally, the assumption that is used to calculate the damage parameters in the final cycle in ICM test is also adopted in this section (see Figure 6(b)). The two different damage evolution stages determined in the ICM test and the change trends for the damage parameters (D_1, D_2, D_3 D_v D_e and D_{AE}) in these two stages also apply to the test results in the ICMM test. A large number of the trans-granular and inter-granular fractures also account for the failure of the specimen B32 (see Figure 9(b)), similar to that of specimen B1 in the ICM test. Here, the main differences between the two cyclic unloading tests are presented.

As shown in Figure 8(b), when the irreversible strain increments exhibit the upward trend, the increments in the irreversible strains and dissipated energy increase slowly in the initial cycles, and then increase rapidly. These initial small changes also occur in the trend for D_{AE} in the rapid damage stage (see Figure 7(b)). In the rapid damage stage in the ICMM test, the rapid increase in the damage parameters concentrates more in the last five cycles compared to the results of the ICM test. This behavior can be clearly observed in the AE event properties in Figure 10(b), in which nearly 85% of the AE hits are generated in the last five cycles.

To investigate the abovementioned differences in the ICM and ICMM tests, Figure 11 shows a comparison of the deviatoric stresses and minimum principal stress in each cycle. It is found that the minimum and intermediate principal stresses in each cycle are equal in both tests. The only differences are in the maximum principal stress, that is, the deviatoric stresses. Based on the characteristics of the irreversible strain, dissipated energy and AE events, there exists a boundary point that can divide the damage evolution into the two stages: a gentle damage stage and a rapid damage stage. The deviatoric stress corresponded to the boundary point in the ICM test is greater than that in the ICMM test and is equal to the stress level in the last five cycle in the ICMM test.
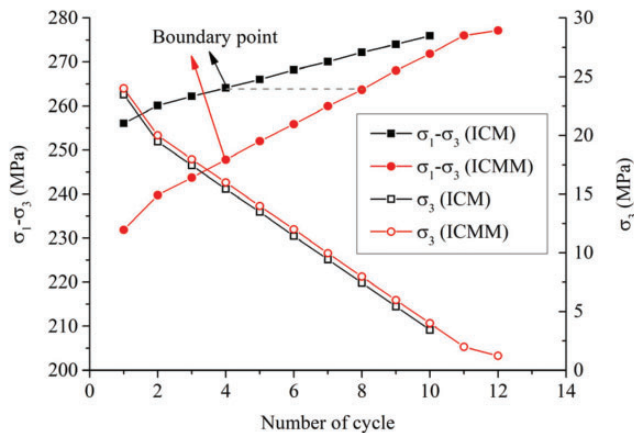

Figure 11. The comparison of the principal stresses in the ICM and ICMM tests.

This stress difference illustrates that the rapid damage stage concentrates more in the last five cycles in the ICMM test.

Discussions

Damage precursor of hard rock based on the evolution characteristics of the strain, energy and AE events

During the construction and maintenance of the deep tunnels, the complex excavation technology, blasting and transport vehicles make it possible for the surrounding rock to be loaded and unloaded repeatedly. From the viewpoint of the entire damage process, the boundary point in this paper can be used as a signal for rock fracturing warnings. The monitoring data for determining the boundary point can be the displacement, which corresponds to the irreversible strains in the three principal stress directions in Figure 8, the stress, which is associated with the characteristic stress level in Figure 11, the AE signals, which are related to the changing trend in Figure 7, and the related energy information (see Figure 8). If possible, using combinations of the displacement, stress, AE event and energy data can increase the accuracy of rock disaster predictions, especially for hard rock under cyclic loading and unloading conditions.

The influence of stress paths on the strength of Jinping marble

The excavation disturbances of an opening in a deeply-buried tunnel are so complicated that they can result in stress redistribution, which is accompanied by stress concentration and the adjustment of the stress paths. Once the stress concentration exceeds the strength of rock material subjected to the corresponding stress path conditions, stress-induced instability may occur. Therefore, it is crucial to investigate the influence of stress paths on the strength of hard rock (Al-Ajmi and Zimmerman, 2005; Chang and Haimson, 2012; Li et al., 2015). Figure 12 shows the strength of Jinping marble in the different loading and unloading tests. In both the ICM test and ICMM test, the predetermined ultimate maximum principal stress σ_1 is equal to 280 MPa. According to the stress paths, the
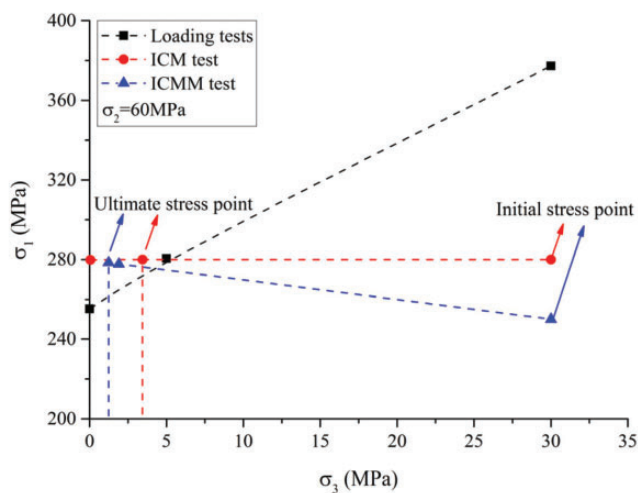

Figure 12. The influence of the stress paths on the strength of Jinping marble.

intersection points with the loading tests are 280 MPa (σ_1) and 5 MPa (σ_3) in the ICM test, and approximately 275 MPa (σ_1) and nearly 4 MPa (σ_3) in the ICMM test. However, the ultimate stresses are 280 MPa (σ_1) and 3.44 MPa (σ_3) for specimen B1, and 280 MPa (σ_1) and 0.05 MPa (σ_3) for specimen B3 in the ICM test. The ultimate stresses are 278.44 MPa (σ_1) and 1.23 MPa (σ_3) for specimen B32, and 277.86 MPa (σ_1) and 1.90 MPa (σ_3) for specimen B27 in the ICMM test. These ultimate stress points are beyond the strength fitted line in the loading tests, which indicates that the strength of rock specimens increases under the unloading conditions. Therefore, it is sensible to provide timely support and to develop appropriate excavation methods for deep tunnels.

Conclusions

To investigate the progressive brittle fracture process of hard rock, two types of true triaxial cyclic loading and unloading tests are performed on Jinping marble. With the aid of AE measuring equipment and SEM technique, the following significant conclusions can be drawn:

1. In both the ICM test and ICMM test, rock damage can be characterized by irreversible strains, dissipated energy, AE signal characteristics and failure patterns. Moreover, the rock damage evolution can be quantified by two damage stages. In the gentle damage stage, the normalized irreversible strains increase linearly, whereas the normalized dissipated energy remains nearly constant. This process is accompanied by a small number of AE hits with low amplitudes. The rapid damage stage is characterized by a nonlinear increase in the normalized irreversible strains. This process is associated with a large number of AE hits with high amplitudes. The dissipated energy in the rapid damage stage increases rapidly. Trans-granular and inter-granular fractures account for the failure of the tested specimens in the unloading tests, thus illustrating the brittle failure patterns of these specimens.
2. The rapid damage stage in the ICMM test is mainly concentrated in the last five cycles. This behaviour can be illustrated by the differences in the deviatoric stresses in each cycle.
3. The boundary point that divides the damage process can be used as the damage precursor signals for warning rock failure. Compared with the strength observed in the loading tests, the unloading process increases the strength of hard rock. Thus, it is crucial to choose the appropriate time for support in deep tunnels.

Declaration of conflicting interests

Funding

ORCID iDs

Yaohui Gao ⬛ https://orcid.org/0000-0002-8743-6733
Zhaofeng Wang ⬛ https://orcid.org/0000-0002-5984-4094

References

Al-Ajmi AM and Zimmerman RW (2005) Relation between the Mogi and the Coulomb failure criteria. *International Journal of Rock Mechanics and Mining Sciences* 42(3): 431–439.

Brace WF, Paulding BW and Scholz C (1966) Dilatancy in the fracture of crystalline rocks. *Journal of Geophysical Research* 71(16): 3939–3953.

Cai M (2008) Influence of intermediate principal stress on rock fracturing and strength near excavation boundaries – Insight from numerical modeling. *International Journal of Rock Mechanics and Mining Sciences* 45(5): 763–772.

Carpinteri A, Lacidogna G, Corrado M, et al. (2016) Cracking and crackling in concrete-like materials: A dynamic energy balance. *Engineering Fracture Mechanics* 155: 130–144.

Chang C and Haimson B (2012) A failure criterion for rocks based on true triaxial testing. *Rock Mechanics and Rock Engineering* 45(6): 1007–1010.

Diederichs MS, Kaiser PK and Eberhardt E (2004) Damage initiation and propagation in hard rock during tunnelling and the influence of near-face stress rotation. *International Journal of Rock Mechanics and Mining Sciences* 41(5): 785–812.

Du K, Tao M, Li X, et al. (2016) Experimental study of slabbing and rockburst induced by true-triaxial unloading and local dynamic disturbance. *Rock Mechanics and Rock Engineering* 49(9): 3437– 3417.

Eberhardt E, Stead D, Stimpson B, et al. (1998) Identifying crack initiation and propagation thresholds in brittle rock. *Canadian Geotechnical Journal* 35(2): 222–233.

Eberhardt E, Stead D and Stimpson B (1999) Quantifying progressive pre-peak brittle fracture damage in rock during uniaxial compression. *International Journal of Rock Mechanics and Mining Sciences* 36(3): 361–380.

Feng XT, Wu S, Li S, et al. (2016a) Comprehensive field monitoring of deep tunnels at Jinping underground laboratory (CJPL-II) in China. *Chinese Journal of Rock Mechanics and Engineering* 4: 649–657.

Feng XT, Xu H, Qiu SL, et al. (2018) In situ observation of rock spalling in the deep tunnels of the China Jinping underground laboratory (2400 m depth). *Rock Mechanics and Rock Engineering* 51(4): 1193–1213.

Feng XT, Xu H, Yang CX, et al. (2020) Influence of loading and unloading stress paths on the deformation and failure features of Jinping marble under true triaxial compression. *Rock Mechanics and Rock Engineering* 53(7): 3287–3301.

Feng XQ and Yu SW (2010) Damage micromechanics for constitutive relations and failure of microcracked quasi-brittle materials. *International Journal of Damage Mechanics* 19(8): 911–948.

Feng XT, Zhang XW, Kong R, et al. (2016b) A novel Mogi type true triaxial testing apparatus and its use to obtain complete stress–strain curves of hard rocks. *Rock Mechanics and Rock Engineering* 49(5): 1649–1662.

Feng XT, Zhang XW, Yang CX, et al. (2017) Evaluation and reduction of the end friction effect in true triaxial tests on hard rocks. *International Journal of Rock Mechanics and Mining Sciences* 97: 144–148.

Gao YH and Feng XT (2019) Study on damage evolution of intact and jointed marble subjected to cyclic true triaxial loading. *Engineering Fracture Mechanics* 215: 224–234.

Gao YH, Feng XT, Zhang XW, et al. (2018) Characteristic stress levels and brittle fracturing of hard rocks subjected to true triaxial compression with low minimum principal stress. *Rock Mechanics and Rock Engineering* 51(12): 3681–3697.

Gao XS, Zhang GH and Roe C (2010) A study on the effect of the stress state on ductile fracture. *International Journal of Damage Mechanics* 19(1): 75–94.

Haimson B (2007) Micromechanisms of borehole instability leading to breakouts in rocks. *International Journal of Rock Mechanics and Mining Sciences* 44(2): 157–173.

He MC, Miao JL and Feng JL (2010) Rock burst process of limestone and its acoustic emission characteristics under true-triaxial unloading conditions. *International Journal of Rock Mechanics and Mining Sciences* 47(2): 286–298.

Iturrioz I, Lacidogna G and Carpinteri A (2014) Acoustic emission detection in concrete specimens: Experimental analysis and lattice model simulations. *International Journal of Damage Mechanics* 23(3): 327–358.

Ju JW, Yuan KY and Kuo AW (2012) Novel strain energy based coupled elastoplastic damage and healing models for geomaterials – Part I: Formulations. *International Journal of Damage Mechanics* 21(4): 525–549.

Kong R, Feng XT, Zhang XW, et al. (2018) Study on crack initiation and damage stress in sandstone under true triaxial compression. *International Journal of Rock Mechanics and Mining Sciences* 106: 117–123.

Li MY, Cao YJ, Shen WQ, et al. (2018) A damage model of mechanical behavior of porous materials: Application to sandstone. *International Journal of Damage Mechanics* 27(9): 1325–1351.

Li X, Du K and Li D (2015) True triaxial strength and failure modes of cubic rock specimens with unloading the minor principal stress. *Rock Mechanics and Rock Engineering* 48(6): 2185–2196.

Li S, Feng XT, Li Z, et al. (2012) In situ monitoring of rockburst nucleation and evolution in the deeply buried tunnels of Jinping II hydropower station. *Engineering Geology* 137-138(7): 85–96.

Liang Y, Li Q, Gu Y, et al. (2017) Mechanical and acoustic emission characteristics of rock: Effect of loading and unloading confining pressure at the postpeak stage. *Journal of Natural Gas Science and Engineering* 44: 54–64.

Liu DQ, He MC and Cai M (2018) A damage model for modeling the complete stress–strain relations of brittle rocks under uniaxial compression. *International Journal of Damage Mechanics* 27(7): 1000–1019.

Liu S and Xu JY (2015) Analysis on damage mechanical characteristics of marble exposed to high temperature. *International Journal of Damage Mechanics* 24(8): 1180–1193.

Lockner DA, Byerlee JD, Kuksenko V, et al. (1991) Quasi-static fault growth and shear fracture energy in granite. *Nature* 350(6313): 39–42.

Martin CD and Chandler NA (1994) The progressive fracture of Lac du bonnet granite. *International Journal of Rock Mechanics and Mining Sciences & Geomechanics Abstracts* 31(6): 643–659.

Mogi K (1972) Effect of the triaxial stress system on fracture and flow of rocks. *Physics of the Earth and Planetary Interiors* 5: 318–324.

Ortlepp WD and Stacey TR (1994) Rockburst mechanisms in tunnels and shafts. *Tunnelling and Underground Space Technology* 9(1): 59–65.

Qiu SL, Feng XT, Xiao JQ, et al. (2014) An experimental study on the pre-peak unloading damage evolution of marble. *Rock Mechanics and Rock Engineering* 47(2): 401–419.

Su GS, Chen ZY, Woody Ju J, et al. (2019) Experimental study of the dynamically induced rockburst of a rock wall with double free faces. *International Journal of Damage Mechanics* 28(4): 611–637.

Tiwari RP and Rao KS (2007) Response of an anisotropic rock mass under polyaxial stress state. *Journal of Materials in Civil Engineering* 19(5): 393–403.

Zhao J, Feng XT, Zhang XW, et al. (2018) Brittle-ductile transition and failure mechanism of Jinping marble under true triaxial compression. *Engineering Geology* 232: 160–170.